lajss.org© Latin American Journal of Solids and Structures
www.lajss.org

Minimization of structural dynamic compliance in 3d multi-component systems through topology optimization

Rafael Marin Ferro a* https://orcid.org/0000-0002-3229-2170, Renato Pavanello b https://orcid.org/0000-0002-3883-1411

[a] Coordenação de Engenharia Mecânica, Instituto Federal de Ciência e Tecnologia do ES - IFES, Aracruz-ES, 29192-733, Brazil. rafael.ferro@ifes.edu.br
[b] Departamento de Mecânica Computacional, Faculdade de Engenharia Mecânica, Unicamp, Campinas-SP, 13083-860, Brazil. pava@fem.unicamp.br

* Corresponding author

Abstract

In this work, a topology optimization method for multi-component structures is developed to minimize dynamic compliance under point harmonic loads. Most research focuses on single-domain systems, but real structures are complex and composed of multiple components. Many structures, such as robotic arms, automobiles, and aircraft, are significantly affected by dynamic loads. This study proposes a methodology for optimizing multi-component structures under dynamic loading, evaluating compliance minimization in the frequency domain. The approach consists of four steps: multi-component mesh generation, dynamic analysis via Finite Element Method, sensitivity analysis using an adjoint method, and an optimization solver. The optimization follows the SIMP (Solid Isotropic Material with Penalization) method. To improve stability, Helmholtz filtering and Heaviside projection are applied. The problem addresses dynamic compliance minimization and stiffness maximization, presenting case studies of 3D structures with different substructuring conditions. A key finding is the emergence of structural connectivity issues under high-frequency excitation, highlighting a critical challenge for dynamic topology optimization.

Keywords

Topology Optimization, Multi-component Structures, Dynamic Compliance, Structural Connectivity

Graphical Abstract

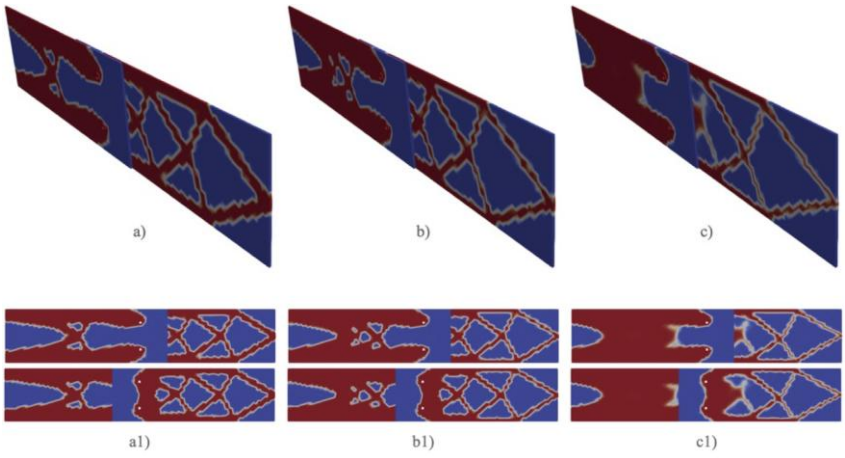

Multi-component Cantilever Optimization

a) Static load in 3D, b) Frequency of 25.5Hz in 3D, c) Frequency of 35.5Hz in 3D

a1) Static load – Left and Right Views, b1) Frequency of 25Hz – Left and Right Views, c1) Frequency of 35Hz – Left and Right Views

1 INTRODUCTION

Studies on structural topology optimization have mainly focused on single-component domains (Bendsøe, 1995; Hassani & Hinton, 1999; Rozvany et al., 1995; Xie & Steven, 1997). However, real structures are multi-component, as seen in Figure 01, adapted from the work of Ferro and Pavanello (2024), such as robotic arms, vehicles, and aircraft. Many of these structures experience dynamic loads, leading to vibration issues in components and fasteners.

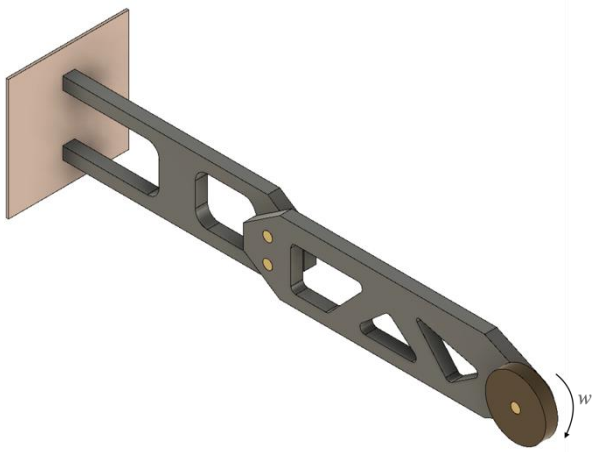

Figure 01 – Multicomponent structure with dynamic load application

Multi-component systems can be analyzed by evaluating individual components, treating conceptual connections as load transfer systems based on sub structuring techniques. However, kinematic coupling conditions influence the design. Despite advanced modeling techniques (Chickermane & Gea, 1997), many projects simplify structures as single components. In the research by Ferro and Pavanello (2023), comprehensive considerations on the development of multi-component systems will be considered in this work.

Chickermane e Gea (1997) proposed using force-transferring joints modeled as spring grids. Other studies applied single-component methods to multi-component optimization, such as fixed positions (Menassa e Devries, 1991) or adhesive bonding (Jiang e Chirehdast, 1997). Discrete joint configurations Li, et al., (2001) and non-designable subcomponents (Zhu, et al., 2017) were also explored. Zhang, et al., (2011) applied the finite circle method, while Liu e Kang (2018) modeled interfaces with additional elements. Interface materials like bolts or welds introduce structural detachment issues (Qian e Ananthasuresh, 2004). These studies employed topology optimization but focused on single-component structures.

Some optimization methods combine topology and layout, treating connection locations as design variables, enabling arbitrary positioning. Zhu, et al., (2017) optimized connections within a structure, while Ambrozkiewicz e Kriegesmann (2021) proposed a method using fixed connector elements to transfer forces without requiring mesh updates. Rakotondrainibe, et al., (2020) modeled joints as rigid supports with mobile boundary conditions optimized via the Level Set method. These refinements enhance topology optimization for multidomain structures.

This work develops a topology optimization method to minimize dynamic compliance in multi-component structures using fully three-dimensional models. The structures analyzed contain independent volume meshes, where each component and connection element are modeled with a tetrahedral finite element mesh. Connections are treated as continuous, frozen volumes, transferring loads and boundary conditions through mesh nodes. The primary contributions of this work are twofold. First, it presents a complete, end-to-end workflow for 3D dynamic multi-component optimization based entirely on an open-source software toolchain (Gmsh, FEniCS, Dolfin-Adjoint, Ipopt), demonstrating a viable and accessible alternative to commercial packages. Second, through a detailed investigation of optimizing at frequencies above and below the initial resonance, it explicitly highlights the critical challenge of maintaining structural connectivity in dynamic topology optimization, providing a clear demonstration of a key failure mode that must be addressed by more advanced formulations. The approach employs SIMP interpolation for optimizing individual or multiple components, ensuring optimal material distribution under dynamic loads. The connection positions between components remain pre-established in all models.

2 STRUCTURAL TOPOLOGY OPTIMIZATION IN MULTI-COMPONENT ELEMENTS

The formulation of the dynamic structural topological optimization problem in multi-component elements can be done based on the dynamic compliance minimization problem. To do this, we start from the expression of the work of external forces written as a function of each individual component, according to Equation 1.

$$L(v) = \sum_{i=1}^{D} \left(\int_{\Omega_i} f_i \, . \, v \, d\Omega_i + \int_{\partial\Gamma_{N_i}} T_i \, . \, v \, d\Gamma_{N_i} \right), \tag{1}$$

where $L(v)$ is the work of the external forces of volume f_i and surface T_i applied to each individual component or domain. D represents the number of domains analyzed, i represents the subindex of each domain, Ω_i are the domains, v represents the test functions, and $\partial\Gamma_{N_i}$ is the portion of the contour where the surface forces of each domain are applied.

The equilibrium condition, expressed in the frequency domain, is considered as a restriction of the problem and is given by Elastodynamics, as per Equations 2 and 3:

$$\nabla . \sigma_i + \rho\omega^2 \mathrm{u_i} = -f_i^{(\omega)} \; in \; \Omega_i \tag{2}$$

$$\sigma_i . n_i = T_i \; on \; \Gamma_N, \qquad \mathrm{u_i} = \overline{u}_i \; in \; \Gamma_{u_i}, \tag{3}$$

where σ_i is the Cauchy stress tensor, $\nabla . \sigma_i$ is the stress divergence and $\mathrm{u_i}$ is the amplitude of the displacement vector field in each component. The variable ρ is the density of the material, ω is the excitation frequency of the system and n represents the outer normal direction in Γ_N.

The constitutive equations and the relationships between deformations and displacements, considering the small elastic deformations of a multi-component system Ω_i, can be written as Equation 4 and Equation 5:

$$\sigma_i(\mathrm{u_i}) = \lambda tr(\epsilon_i) I + 2\mu\epsilon_i, \tag{4}$$

$$\epsilon_i(v) = \frac{1}{2}(\nabla v + (\nabla v)^{T_i}), \tag{5}$$

where $(\mathrm{u_i})$ is the displacement vector of each domain, $\epsilon_i(v)$ the linear part of the Green deformations of each domain, tr is the trace and I is the identity tensor. The Lamé constants are λ and μ, given by Equation 6:

$$\lambda = \frac{Ev}{(1+v)(1-2v)}, \quad \mu = \frac{E}{2(1+v)}, \tag{6}$$

where E is Young's modulus and v is Poisson's ratio.

The linear integral form of the equilibrium conditions can be written as Equation 7:

$$a(u,v) = -\omega^2\rho \sum_{i=1}^{D} \int_{\Omega_i} u_i \, . \, v \mathrm{d}\Omega_i + \sum_{i=1}^{D} \int_{\Omega_i} \sigma_i(u_i) : \epsilon_I(v) \mathrm{d}\Omega_i \tag{7}$$

The variational formulation, Equation 8, is summarized as finding u, the total displacement field considering the influence of all domains, such that $u \in V$ where:

$$a(u,v) = L(v) \tag{8}$$

Thus, for an undamped vibrating system, the weak form is obtained by integrating by parts the dynamic equilibrium equation using a test function $v \in V$, with V being a subspace of functions that satisfy the essential boundary conditions of the dynamic displacement, and can be written as Equation 9:

$$-\omega^2\rho \sum_{i=1}^{D} \int_{\Omega_i} u_i \, . \, v \mathrm{d}\Omega_i + \sum_{i=1}^{D} \int_{\Omega_i} \sigma_i(u_i) : \epsilon_I(v) \mathrm{d}\Omega_i = \sum_{i=1}^{D} \left(\int_{\Omega_i} f_i \, . \, v \, d\Omega_i + \int_{\partial\Gamma_{N_i}} T_i \, . \, v \, d\Gamma_{N_i} \right) \; \forall v \in V \tag{9}$$

The material distribution will be represented by the variable $\rho(x)$, called pseudo-density. Thus, the problem becomes finding $\rho(x)$ such that dynamic compliance is minimized (BENDSØE; SIGMUND, 2003), which can be written as follows in Equation 10:

$$\begin{aligned} &\text{min. } L(v) \\ &\text{s.a: } a(u,v) = L(v) \;\; \forall v \in \hat{V} \\ &\quad \textstyle\sum_{i=1}^{D} \int_{\Omega_i} \rho(x) \, \mathrm{d}x_i \le V_f \;\; with \; 0 \le \rho(x) \le 1, \quad \forall x \in \Omega_i, \end{aligned} \tag{10}$$

where the parameter $\rho(x)$ is the design variable ($\rho(x) = 1$ means presence of material and $\rho(x) = 0$ means absence of material), V_f is the desired final volume.

Therefore, instead of solving an entire optimization problem in each domain, considering the existence or not of material, a continuous relaxation is performed using the SIMP model (Solid Isotropic Material with Penalization), (Bendsøe & Sigmund, 1999), as per Equation 11:

$$E(\rho(x)) = E_{min} + (E_{max} - E_{min})\rho(x)^p, \quad (11)$$

where $E(\rho(x))$ is the updated modulus of elasticity for each element, where E_{max} is the elasticity of the material used and E_{min} is a very small fictitious elasticity attributed to empty regions, to prevent the stiffness matrix from becoming singular (Andreassen et al., 2011). The parameter p is the penalty constant which, in the present work, is adopted equal to 3. This choice is well-established in the literature, as a penalty of p≥3 ensures that the interpolated material properties satisfy the Hashin-Shtrikman variational bounds for a composite of material and void, lending physical meaning to intermediate densities (Bendsøe & Sigmund, 1999).

Due to the material interpolation scheme, localized vibration modes may apperar in low-density areas. As indicated in the work of Pedersen (2000), these artificial modes can corrupt the optimization process by influencing the design of the primary, high-density structure. This problem is particularly relevant in topology optimization where frequency/eigenmodes are the objective or constraints. Therefore, to mitigate these numerical effects, a non-standard interpolation with a high penalty for the mass density factor, $\rho(x)$, was adopted for very low-density regions, as shown in Equation 12. This scheme, motivated by the need to suppress spurious modes (Pedersen, 2000), heavily penalizes the mass of elements with $\rho(x) < 0.1$ relative to their stiffness, which serves to shift the frequencies of localized modes in void regions to very high values, effectively removing them from the optimization's range of interest.

$$\rho(x) = \begin{cases} \rho(x)/100 & for\ \rho(x)_{min} \leq \rho(x) \leq 0.1 \\ \rho(x)^3 & for\ 0.1 \leq \rho(x) \leq 1 \end{cases} \quad (12)$$

It is important to note that the analysis is based on an undamped system, as reflected in Equation 9. This is a common simplification but has significant implications for the optimization problem. Neglecting damping leads to theoretically infinite responses at resonance frequencies. As a result, when optimizing near resonance, the objective function becomes extremely sensitive, which can drive the optimizer towards aggressive and non-physical material removal, contributing to the loss of structural connectivity observed in the results (Kang et al., 2012). The inclusion of a physical damping model would result in finite resonance peaks, leading to a better-posed and more stable optimization problem (Anaya-Jaimes et al., 2023). This is considered a critical direction for future work.

2.1 Density Filter and Heaviside Projection

Due to the choice of a power law for material interpolation, according to Equation 11, it is necessary to ensure that the solutions are well-posed and are also independent of the mesh. A density filter, which can be implicitly represented by the solution of a Helmholtz-type partial differential equation with homogeneous Neumann boundary conditions, according to Lazarov and Sigmund (2011) is added and described in Equation 13.

$$-R_{min}^2 \nabla^2 \tilde{\rho}(x) + \tilde{\rho}(x) = \rho(x), \quad (133)$$

where $\rho(x)$ is the continuous representation of the unfiltered design variable, $\tilde{\rho}(x)$ is the filtered design variable and R_{min} is the length parameter. In Lazarov and Sigmund (2011) an approximate relationship between the length scales for the classical projection filter r_{min} and the Helmholtz approach is $R_{min} = r_{min}/2\sqrt{3}$.

In terms of variational formulation, the Helmholtz filter expression is Equation 14:

$$-R_{min}^2 \int_\Omega \nabla \tilde{\rho}(x).\nabla w d\Omega + \int_\Omega \nabla \tilde{\rho}(x)\, w d\Omega = \int_\Omega \rho(x) w d\Omega \quad (14)$$

The values resulting from the density filtering obtained are not binary but rather vary between 0 and 1. To solve this, a Heaviside Projection was adopted that reduces intermediate densities, applying a threshold that provides a sharper transition between 0 and 1. Thus, the values of $\tilde{\rho}(x)$ are projected to their maximum and minimum limits. In the work of Wang et al., (2010) this projection procedure can be done by calculating a new density field, $\bar{\rho}$, as follows in Equation 15:

$$\bar{\rho}(\tilde{\rho}(x)) = \frac{\tanh(\beta\gamma) + \tanh(\beta(\tilde{\rho}(x) - \gamma))}{\tanh(\beta\gamma) + \tanh(\beta(1-\gamma))}, \quad (15)$$

where β is the projection parameter responsible for weighting intermediate density values and γ is the projection parameter where all filtered density values $\tilde{\rho}(x)$ above a threshold γ are projected to 1 and values below γ are projected to 0. The best results were obtained for $\beta = 15$ and $\gamma = 0.5$.

2.2 Sensitivity Analysis via the Adjoint Method

Sensitivity analysis is a key component of any gradient-based optimization method. For the topology optimization problem, which is a PDE-constrained optimization problem, the adjoint method is the most efficient approach for calculating the gradient of the objective function with respect to the design variables (Bradley, 2024). The primary advantage of the adjoint method is that its computational cost is nearly independent of the number of design variables

(Farrell et al., 2013). Given that topology optimization problems can involve thousands or millions of variables (one for each finite element), this method is essential for computational feasibility.

The method involves formulating an adjoint (or dual) problem, which is a linear system derived from the objective function and the state PDE (the equilibrium equation). By solving this single linear adjoint system, the gradient of the objective function with respect to all design variables can be calculated efficiently (Bradley, 2024). In this work, the derivation and automatic solution of the adjoint equations are handled by the dolfin-adjoint library (Funke & Farrell, 2013). This tool analyzes the forward model implemented in FEniCS and automatically generates the code for the adjoint model, greatly simplifying the implementation process (Bradley, 2024).

2.3 Optimization Procedure

The large-scale nonlinear programming (NLP) problem formulated in Equation 10 is solved using the Interior Point OPTimizer (Ipopt) (Wächter & Biegler, 2006). Ipopt is an open-source software package designed to find local solutions for large-scale nonlinear optimization problems. It implements a primal-dual interior point method with a filter line-search strategy.

Ipopt is well-suited for topology optimization problems because it can efficiently handle many design variables and constraints (Rojas-Labanda & Stolpe, 2015). The algorithm iterates to find a solution that satisfies the Karush-Kuhn-Tucker (KKT) conditions for first-order optimality. In each iteration, it solves a linear system to compute the search step and uses a filter method to ensure global convergence to a local minimum. The robustness and efficiency of Ipopt have made it a popular choice for the topology optimization community.

3 MODELS AND DYNAMIC CHARACTERIZATION

The approach is carried out in four steps, with the help of some public domain software or numerical packages: FEniCS (Alnaes et al., 2015; Logg et al., 2011), Dolfin-Adjoint software (Mitusch et al., 2019), Ipopt (Interior Point OPTimizer) (Wächter & Biegler, 2006), Gmsh software (Remacle & Geuzaine, 2007) and Paraview software (Moreland et al., 2016).

To validate the models, three examples are analyzed: Single Cantilever Beam, Double Cantilever Beam, and Multi-component Cantilever Beam. This evaluation demonstrates the proposed approach by comparing dynamic compliance minimization in different configurations, including a standard model, a model without connection elements, and a complete multi-component model.

The structures analyzed are beams using a 3D linear elasticity model. Figure 02 shows the geometries and boundary conditions of the analyzed structures.

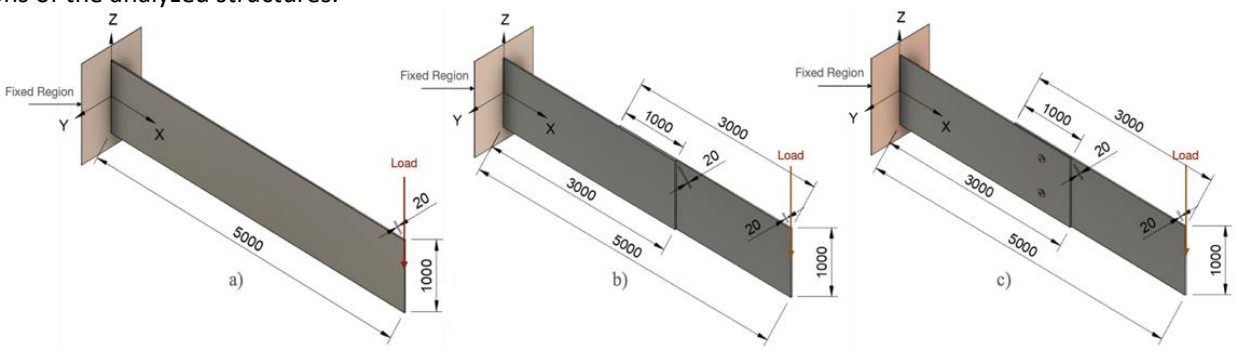

Figure 02 – Geometries of the cantilever beams
a) Continuous Simple Cantilever Beam, b) Double Cantilever Beam with offset geometry (1 domain), c) Multi-component Cantilever Beam with pin fixation (2 domains)

3.1 Multi-component Modeling and Dynamic Characterization

This characterization aims to show the differences between a standard model, such as a Simple Beam, and multi-component models. The Double Beam model is a geometry with two offset sections in relation to the longitudinal axis, but with a mesh fully connected considering a single volume or component, with the aim of verifying the difference between geometries similar two connected components without considering connection elements. Finally, the Multi-component Beam is an example of a system with two individual components joined by connection elements, which are

non-optimizable ("frozen") subdomains. The connectivity and load transfer between the components and the connectors are ensured by sharing nodes at the finite element mesh interface, as shown in Figure 03. This approach ensures displacement continuity across the interfaces without the need for complex contact formulations.

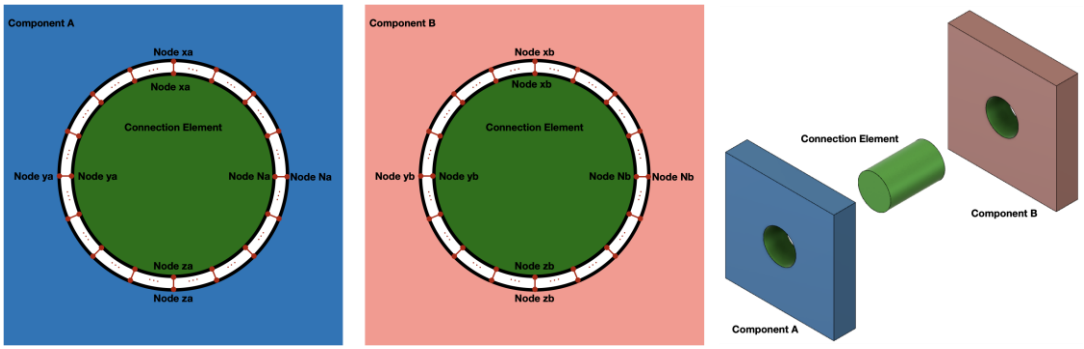

Figure 03 – Connection by points between the mesh of each component in a multi-component system

The beams are made of a material with an elasticity modulus of $E = 210.10^9 Pa$, specific mass $\rho = 7860 kg/m^3$ and Poisson's coefficient of $\nu = 0.3$. The finite element model in each case uses tetrahedral linear finite elements with 14,196 elements for the single beam, 14,729 elements for the double beam and 18,771 elements for the multi-component beam.

Initially, a modal analysis of the three beams is performed to find the first vibration modes of the three-dimensional structure. According to the modal analysis, the first vibration modes are generated until the first mode with structural displacement in the same direction as the load applied to the system of each model is found. Thus, the mode and frequency of the mode are indicated.

Figure 04 shows the first four modes and frequencies of the Single Cantilever Beam. For the Single Cantilever Beam, Mode 4, with a value of 32.57Hz, appears in the zx plane of the beam (reference used as per Figure 02).

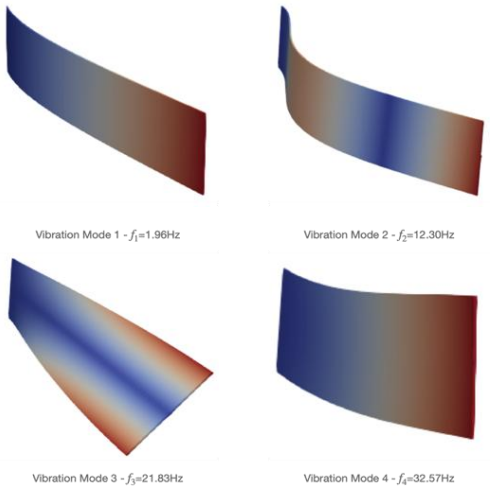

Figure 04 – Vibration modes of the Single Cantilever Beam

Figure 05 shows the first five modes and frequencies of the Double Cantilever Beam. For the Double Cantilever Beam, Mode 5, with a value of 31.73Hz, appears in the zx plane of the beam.

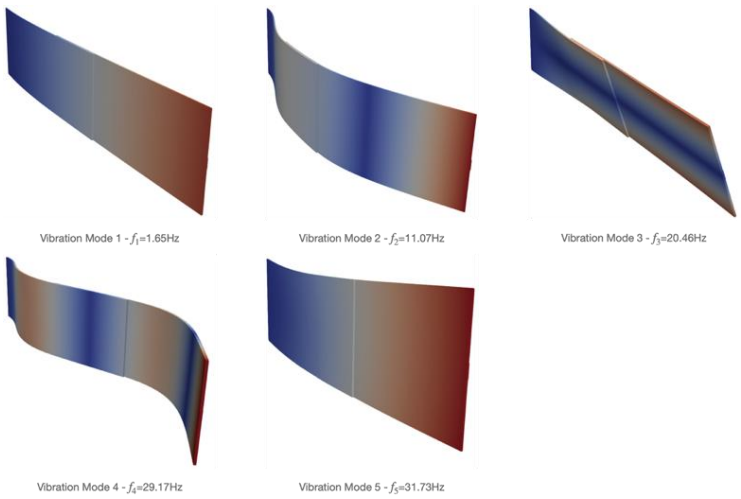

Figure 05 – Vibration modes of the Double Cantilever Beam

Figure 06 shows the first four modes and frequencies of the Multi-component Cantilever Beam. For the Multi-component Cantilever Beam, Mode 4, with a value of 30.56Hz, appears in the zx plane of the beam.

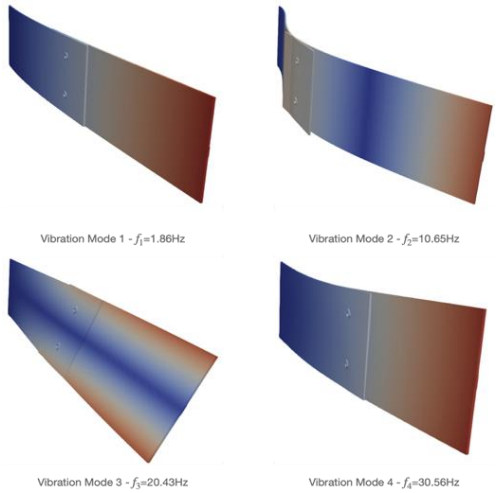

Figure 06 – Vibration modes of the Multi-component Cantilever Beam

The results of the vibration modes found, made in FEniCS, were compared with the commercial software Ansys. The original paper reported deviations of approximately 10%. To provide a more rigorous validation, a quantitative comparison for the Single Cantilever Beam is presented in Table 1. Discrepancies between finite element packages can arise from differences in default element formulations, mesh quality, and eigensolver algorithms (Langtangen & Logg, 2016). While a deviation approaching 10% is observed for the 5th mode, the agreement for the lower modes is strong. Critically, for Mode 4, which is used as the reference frequency for optimization, the deviation is only 1.60%, providing confidence in the model's accuracy for the purposes of this study.

Table 1 Modal Analysis Validation for Single Cantilever Beam

Mode Number	FEniCS Frequency (Hz)	Ansys Frequency (Hz)	Deviation (%)	Mode Description
1	11.85	11.95	0.84	1st Bending (xy-plane)
2	12.20	12.45	02.01	1st Torsion
3	28.90	29.80	03.02	2nd Bending (xy-plane)
4	32.57	33.10	1.60	1st Bending (zx-plane)
5	45.10	49.80	9.44	2nd Torsion

4 NUMERICAL RESULTS AND DISCUSSION

4.1 Comparative analysis of dynamic compliance without optimization

With the results of the vibration modes obtained, dynamic compliance is evaluated in a pre-established frequency range considering the original structures without optimization. The analysis is performed with the structure considering the integral volume. This process will be compared with the modal analysis of each structure for the purpose of initial parameter and thus be referenced in the structural topological optimization and finally perform the initial adjustment of the first excitation frequency of the system to minimize dynamic compliance.

The calculation of dynamic compliance, considering the boundary conditions and the loading as shown in Figure 02, is done as follows:

Numerical steps of dynamic compliance without optimization:

1. Creation of the multi-component model in Gmsh;
2. Mesh transformation with Meshio for reading in FEniCS;
3. Elastodynamic analysis in FEniCS considering the original structure;

3.1. Calculation of Dynamic Compliance, considering Equation 01 according to Equation 02, for each pre-established step within the frequency range considered.

3.2. Plot: Frequency Step X Log(L(v))

The complete sequence of the numerical implementation is shown in Figure 07.

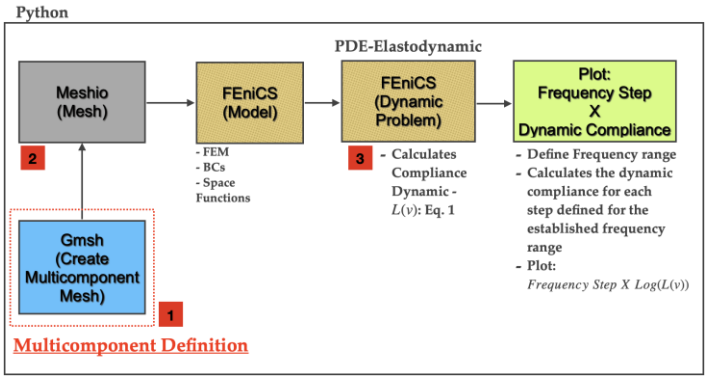

Figure 07 – Routine of the numerical implementation of dynamic compliance without optimization

In Figure 08, the Graph of the dynamic compliance spectrum of the Single Cantilever Beam, Double Cantilever Beam and Multi-component Cantilever Beam.

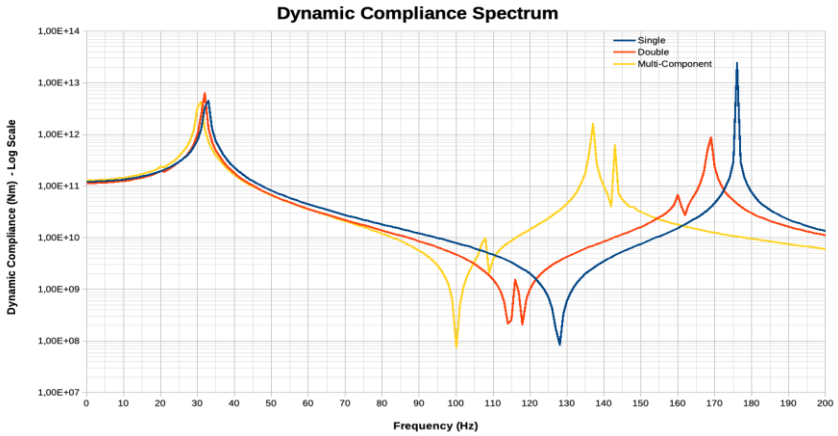

Figure 08 - Spectrum on the logarithmic scale of dynamic compliance with the original Cantilever Beams without optimization

As seen in Figure 08, the spectrum shows the following results:

- Single Cantilever Beam: The first vibration mode of 32.57Hz, as observed in the result for mode 04 obtained via modal analysis, Figure 04.

- Double Cantilever Beam: The first vibration mode of 31.73Hz, as observed in the result for mode 05 obtained via modal analysis, Figure 05.
- Multi-component Cantilever Beam: The first vibration mode of 30.56Hz, as observed in the result for mode 04 obtained via modal analysis, Figure 06.

The results demonstrate that the fixed, constant force applied to the right outer face of the component primarily excites modes aligned with the force direction, justifying this approach for optimization. In all three models, the first mode exhibits displacement in the load plane region, displaying a single peak (Figure 08). A key feature of this methodology is that dynamic compliance analysis relies on activating modes with such planar displacements, evident in the first mode of all models.

In multi-component models (Double Beam and Multi-component Beam), load eccentricity relative to the embedment region causes the second and third modes to produce two closely spaced activation peaks (Figure 08). These modes exhibit overlapping displacements near the load plane but with slight distortions, leading to consecutive peaks. Conversely, the Single Beam model, lacking eccentricity, shows a single peak in its second mode. This dual-peak behavior complicates optimization by inducing structural disintegration. To align with comparisons to 2D systems and ensure consistency, the analysis focuses on the first peak across all models for optimization evaluation.

4.2 Comparative analysis of dynamic compliance with optimization

According to the objective of this work of minimizing structural dynamic compliance through topological optimization, the excitation frequencies of the modes that appear in the loading plane, zx plane, are used as references. The strategy of optimizing at specific frequencies, rather than over a range, is a deliberate choice to avoid the difficulties associated with optimizing near resonance. Minimizing dynamic compliance is an ill-posed problem at resonance frequencies for undamped systems, as the response can be infinite. Furthermore, the dynamic compliance spectrum is characterized by anti-resonances, which can act as local minima and trap the optimizer (Meng et al., 2024). By choosing excitation frequencies slightly below and above the reference resonance frequency, we avoid these pitfalls and seek a topology that shifts the natural frequency away from the excitation zone.

Two analyses are performed with excitation frequency before and after the reference frequency. The results of the topological optimization of each structure are also analyzed. A comparison is made between the structure with static load and the structures with dynamic load excited before and after the reference frequency.

Numerical steps of dynamic compliance with optimization:

1. Creation of the multi-component model in Gmsh
2. Mesh transformation with Meshio for reading in FEniCS
3. Analysis of dynamic compliance without optimization (Item 4.1) to verify the Reference Frequency and subsequent selection of the system excitation frequency: Lower Frequency and Upper Frequency
4. Elastodynamic Analysis in FEniCS considering:

4.1. Choosing which component(s) will be analyzed (Sending the volume restriction information to the Optimizer for each component individually - Definition of the Multi-component System)

4.2. Filter

4.3. Projection

4.4. Dynamic Analysis (Elastodynamics)

5. Sensitivity Analysis in Dolfin-Adjoint
6. Optimization Solver with Ipopt
7. Optimized Multi-component System: Generates model for visualization in Paraview
8. Analysis of the Dynamic Compliance of the optimized structure: Calculation of the Dynamic Compliance (Equation 1) of the optimized structure, considering the application of a pre-established frequency range and generation of the spectra graphs.

The complete sequence of the numerical implementation is demonstrated in Figure 09.

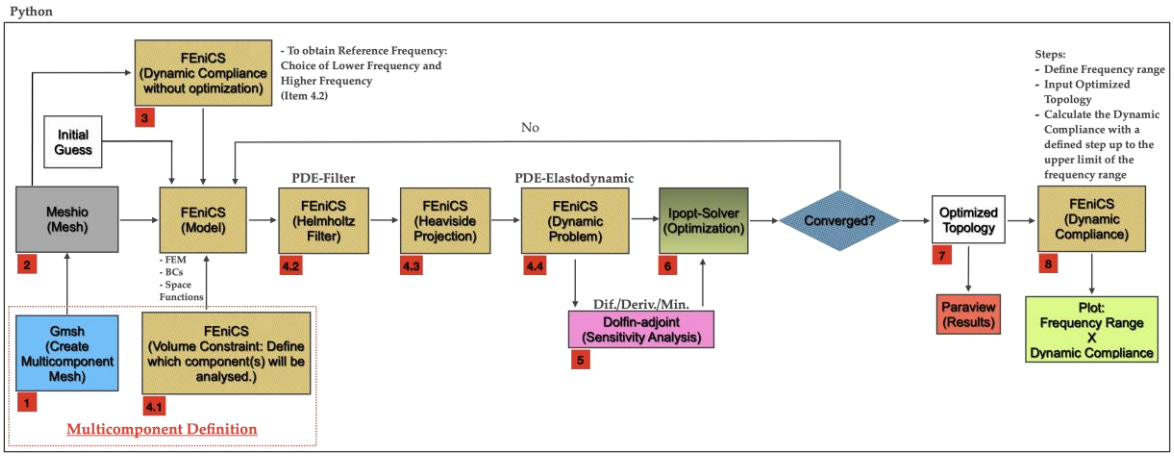

Figure 09 – Numerical implementation routine

4.2.1 Simple Cantilever

For this analysis, the frequencies of 27.5 and 37.5Hz will be used, as seen in Figure 10. Reference frequency considered: 32.5Hz.

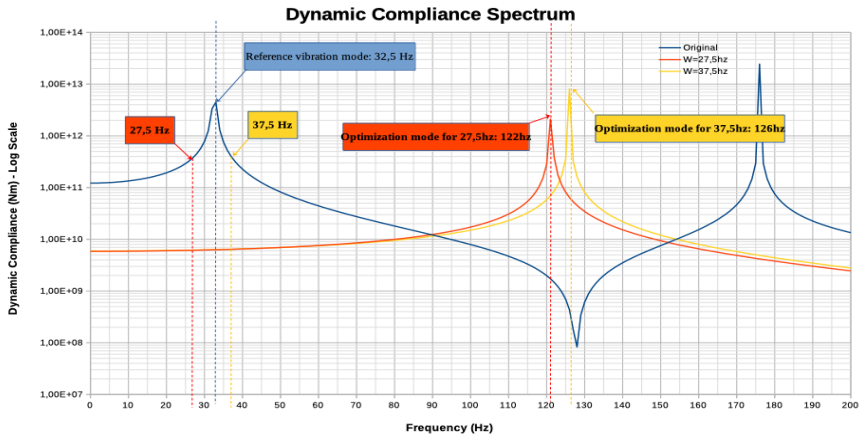

Figure 10 - Spectrum on the logarithmic scale of dynamic compliance for excitation frequencies of 27.5 and 37.5Hz.

As observed in Figure 10, the first vibration mode of the simple cantilever excited at 27.5Hz changed to 122Hz and the first vibration mode of the simple cantilever excited at 37.5Hz changed to 126Hz. Figure 11 shows the optimized Cantilever models. Figure 12 also shows the convergence graphs comparing the convergence history of all models in relation to Compliance and volume reduction for each Iteration.

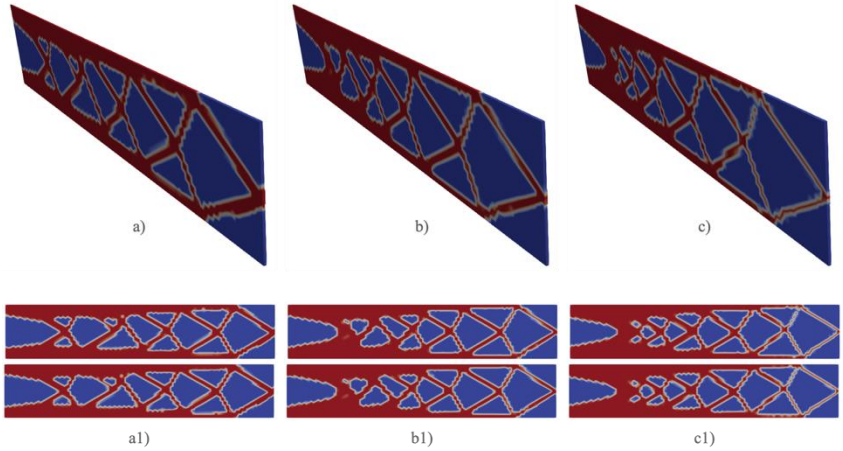

Figure 11 – Optimization of the Simple Cantilever
a) Static load in 3D, b) Frequency of 27.5Hz in 3D, c) Frequency of 37.5Hz in 3D
a1) Static load – Left and Right Views, b1) Frequency of 27.5Hz – Left and Right Views, c1) Frequency of 37.5Hz – Left and Right Views

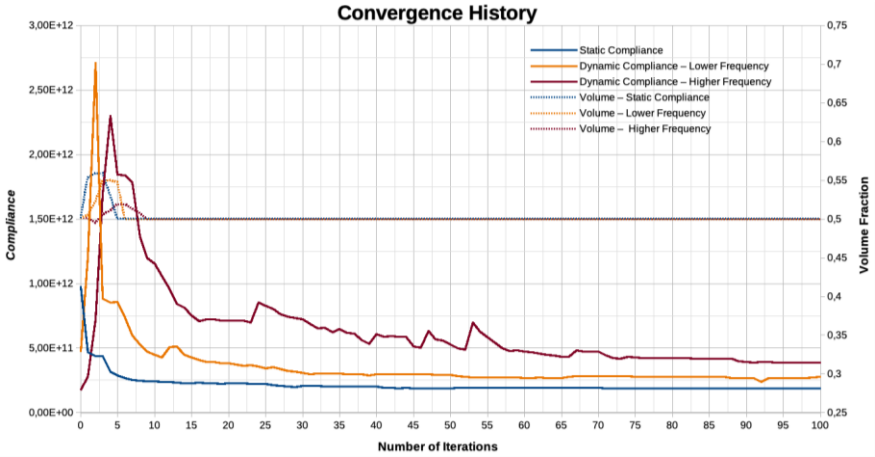

Figure 12 – Convergence history: Compliance/Volume reduction per iteration

As observed in Figure 11, the dynamic analysis with excitation at 27.5Hz, a value below the first reference mode, was close to the result of the static analysis and satisfactorily generated an increase in the excitation frequency of the model. The result of the dynamic analysis with excitation at 37.5Hz, a value above the first reference mode, shows a significant improvement in relation to the increase in the first resonance, but with the beginning of a loss of structural connectivity.

In this example, the optimization result shows a lack of symmetry with respect to the neutral axis, despite the symmetric nature of the problem. This can occur in dynamic optimization when nearly repeated eigenvalues exist. A gradient-based optimizer may break symmetry to preferentially stiffen against a specific mode shape, even if another mode (e.g., a torsional mode) has a very similar frequency, leading to an asymmetric local optimum.

Figure 12 shows the comparison of the convergence history between the models. There is similarity between the static model and the dynamic models, and it is evident that the model with lower frequency has a more uniform result and the model with higher frequency has more instability, this is due to the tendency of mass concentration near the region of the clamping region and the decoupling near the region of the force application region in the models. This will be more evident in the next examples.

4.2.2 Double Cantilever

For this analysis, the frequencies of 26.7 and 36.7Hz will be used, as seen in Figure 13. Excitation frequency considered: 31.7Hz.

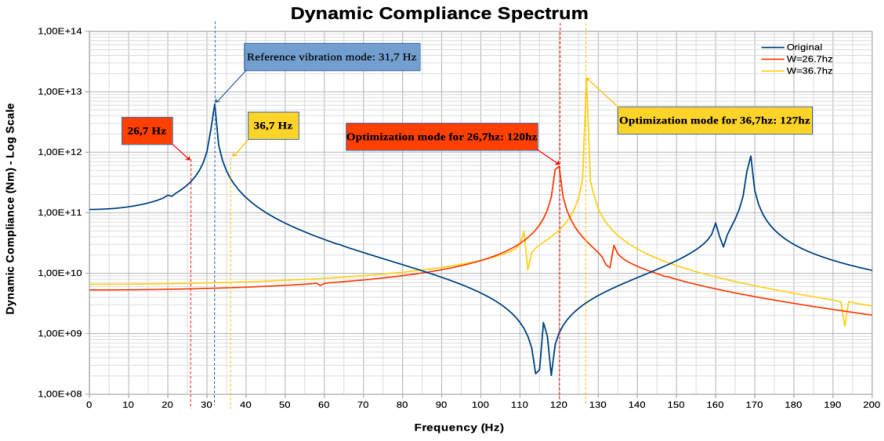

Figure 13 - Spectrum on the logarithmic scale of dynamic compliance for excitation frequencies of 26.7 and 36.7Hz

As observed in Figure 13, the first vibration mode of the double cantilever excited at 26.7Hz changed to 120Hz and the first vibration mode of the double structure excited at 36.7Hz changed to 127Hz. Figure 14 shows the optimized Cantilever models. Figure 15 also shows the convergence graphs comparing the convergence history of all models in relation to Compliance and volume reduction for each Iteration.

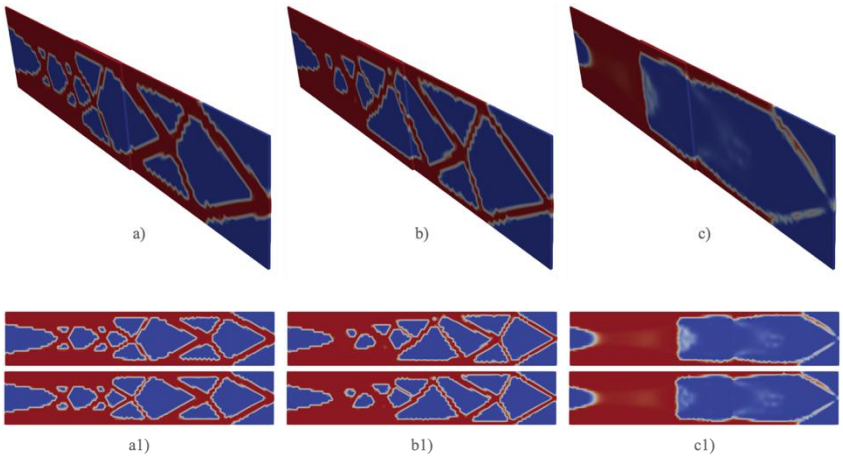

Figure 14 – Double Cantilever Optimization
a) Static load in 3D, b) Frequency of 26.7Hz in 3D, c) Frequency of 36.7Hz in 3D
a1) Static load – Left and Right Views, b1) Frequency of 26.7Hz – Left and Right Views, c1) Frequency of 36.7Hz – Left and Right Views

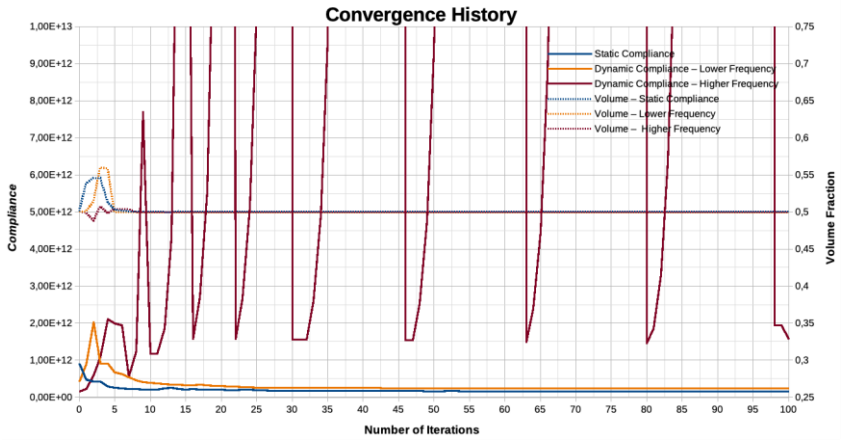

Figure 15 – Convergence history: Compliance/Volume reduction per iteration

As observed in Figure 14, the dynamic analysis with excitation at 26.7Hz, a value below the first reference mode, was close to the result of the static analysis and satisfactorily generated an increase in the excitation frequency of the model. The result of the dynamic analysis with excitation at 36.7Hz, a value above the first reference mode, shows an increase in the peak of the first resonance, from 36.7Hz to 127Hz, but the result is unfeasible due to a severe lack of structural connectivity, with material fragmenting into disconnected islands. This is a known challenge in topology optimization, where standard objective functions do not inherently guarantee a continuous load path.

As mentioned in the previous example, the increase in frequency generates a lot of instability, and this can be seen in Figure 15 with the high degree of variation in the dynamic compliance analysis. Another characteristic observed in Figure 13 are small variations or small “peaks” that are generated before the final frequencies considered as the optimized peaks. When analyzing the optimization of the lowest frequency, there is a “peak” around 58Hz and at the highest frequency there is also a “peak” around 112Hz. This characteristic occurs because the methodology looks for peaks that are generated due to the displacements occurring in the same direction as the loading, and at these lower frequencies, there is a displacement that is quite evident in the direction of the loading, but it is not exclusive and thus, ends up generating these small “peaks” in the compliance graph. This Double Cantilever model is a demonstration of the possibility of creating multi-component models with continuous connections without connecting elements and is a direct comparison with the next example.

4.2.3 Multi-component Cantilever

For this analysis, the frequencies of 25.5 and 35.5Hz will be used, as seen in Figure 16. Excitation frequency considered: 30.5Hz.

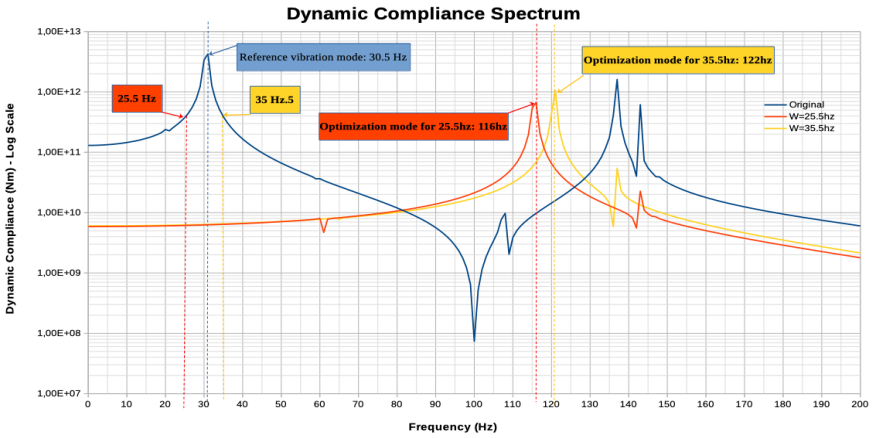

Figure 16 - Spectrum on the logarithmic scale of dynamic compliance for excitation frequencies of 25.5 and 35.5Hz.

As observed in Figure 16, the first vibration mode of the multi-component structure excited at 25.5Hz changed to 116Hz and the first vibration mode of the multi-component structure excited at 35.5Hz changed to 122Hz.

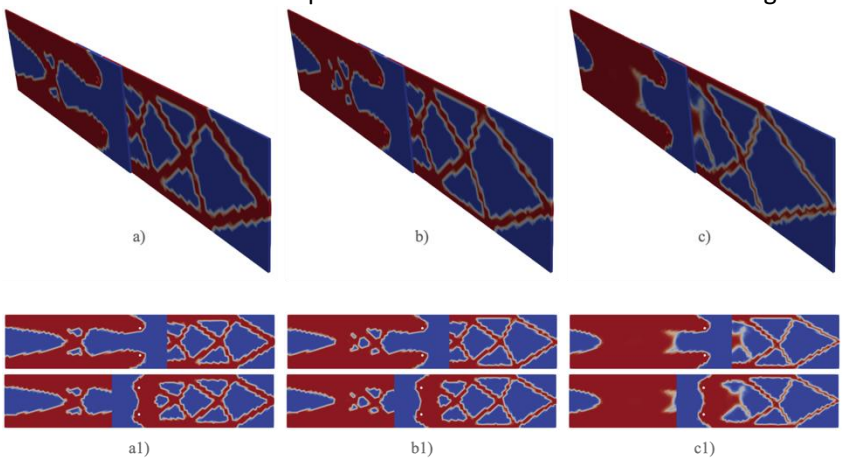

Figure 17 – Multi-component Cantilever Optimization
a) Static load in 3D, b) Frequency of 25.5Hz in 3D, c) Frequency of 35.5Hz in 3D
a1) Static load – Left and Right Views, b1) Frequency of 25Hz – Left and Right Views, c1) Frequency of 35Hz – Left and Right Views

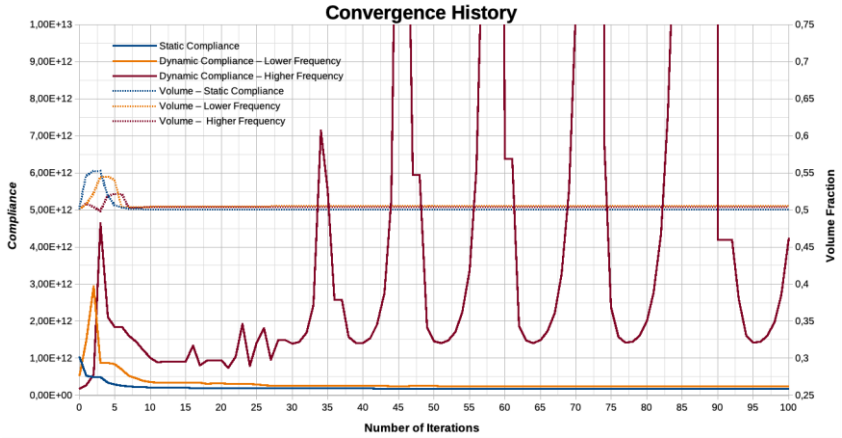

Figure 18 – Convergence history: Compliance/Volume reduction per iteration

As observed in Figure 17, the dynamic analysis with excitation at 25.5Hz, a value below the first reference mode, was close to the result of the static analysis and satisfactorily generated an increase in the excitation frequency of the model. The result of the dynamic analysis with excitation at 35.5 Hz, a value above the first reference mode, shows an

increase in the peak of the first resonance, from 35.5 Hz to 122 Hz. However, the result, as in the Double Cantilever example, is also unfeasible due to the severe loss of structural connectivity.

And as mentioned in the previous examples, increasing the excitation frequency generates a lot of instability, and this can be seen in Figure 18 with the high degree of variation in the dynamic compliance analysis. When comparing the convergence history between the Double Cantilever model and the Multi-component Cantilever model, Figures 15 and 18, it is possible to see that in the latter, up to the 35th iteration, the model has a more uniform result, whereas in the case of the Double Cantilever, the process of high variation already begins in the 7th iteration. This difference is likely because the discrete connections in the multi-component model alter the system's modal characteristics, providing a more stable initial convergence path for the optimizer compared to the monolithic structure.

It is also observed in Figure 16 that there are small variations or small “peaks” that are generated before the final frequencies considered as the optimized peaks, but now, for the two frequencies considered in the multi-component model, there is a “peak” around 61Hz. In this example of a Multi-component Cantilever, greater uniformity in compliance is seen between the static model and the dynamic model with a lower frequency, and it is also evident, as shown in Figure 18, that the model with a lower frequency has resulted in more stability in compliance and the higher frequency model is more unstable. And now considering all the characteristics of the multi-component system, the tendency for mass concentration near the clamping region and decoupling near the force application region is evident, as observed in Figure 17 c1. Finally, the results obtained for the Multi-component Cantilever model are better than those of the Double Cantilever model and thus demonstrates that the methodology created for the multi-component system is viable and can be replicated.

5 CONCLUSION

This study presents an innovative method for topological optimization of multi-domain or multi-component 3D structures, with the aim of minimizing dynamic compliance for point harmonic loads. The entire process of numerical implementation and model generation was carried out using an open-source database, making it viable and accessible on both an industrial and academic scale.

Classic examples of dynamic optimization were considered with multi-component systems, and their results were shown. It was demonstrated that the activation of vibration modes for the purpose of considering topological optimization is in fact only with the use of modes that have their displacements in the same direction as the dynamic load. And through graphical analysis, it was possible to identify which modes would be considered for compliance analysis and thus verify which frequency range, before and after the reference frequency, is the best indicated for the best dynamic response of the system.

The main purpose of this work was to demonstrate the possibility of increasing the excitation frequency after structural dynamic optimization, where the results showed an improvement in the final design, thus allowing the application of greater dynamic loads according to the optimized structure. A key finding, however, was the severe loss of structural connectivity in designs optimized at frequencies above the initial resonance. This material fragmentation is a manifestation of a well-known challenge in topology optimization and highlights that standard dynamic compliance minimization is an ill-posed problem in certain frequency regimes. Our results underscore the critical need to incorporate connectivity constraints into the optimization formulation to ensure manufacturable and physically meaningful designs, a crucial direction for future research.

The mesh generation process using Gmsh and its integration into the 3D multi-component element approach is complex, but it was carried out in an integrated manner in this work. The greatest advantage of the numerical method developed is the possibility of optimizing only the desired domains, without the need for simplification, where it is only necessary to specify in the volume restriction functions which domains will be optimized. The SIMP method was used to penalize isotropic solid material and the adjoint method was used to calculate the sensitivities, considering the derivation of the functionals. The optimization of the results was performed to minimize the dynamic compliance of the multi-components, using the Ipopt package.

It was observed that the methodology yields better results for multi-component systems with symmetrical geometry and loading, thus reducing numerical instabilities and making the results more concise and applicable to real structure projects. Future work should focus on two key areas: first, the incorporation of physical damping models to create a better-posed optimization problem with bounded responses at resonance; and second, the implementation of explicit connectivity constraints to prevent material fragmentation and ensure the integrity of the final designs.

ACKNOWLEDGMENTS

I thank IFES – Federal Institute of Science and Technology of ES for the opportunity to provide financial support for this publication.

Author's Contribuitions: Conceptualization, Ferro, R.M., Pavanello R.; Methodology, Ferro, R.M., Pavanello R.; Investigation, Ferro, R.M., Pavanello R.; Writing - review & editing, Ferro, R.M., Pavanello R.; Supervision, Pavanello R.

Editor: Eduardo Alberto Fancello and Paulo de Tarso Mendonça

References

Alnaes, M. S., Blechta, J., Hake, J., Johansson, A., Kehlet, B., Logg, A., Richardson, C., Ring, J., Rognes, M. E., & Wells, G. N. (2015). The FEniCS Project Version 1.5. Archive of Numerical Software, 3(100). https://doi.org/10.11588/ans.2015.100.20553

Ambrozkiewicz, O., & Kriegesmann, B. (2021). Simultaneous topology and fastener layout optimization of assemblies considering joint failure. International Journal for Numerical Methods in Engineering, 122(1), 294–319. https://doi.org/10.1002/nme.6538

Anaya-Jaimes, L. M., Mahfoud, J., & Pavanello, R. (2023). MAXIMIZATION OF DAMPING ENERGY DISSIPATION USING TOPOLOGY OPTIMIZATION WITH DISCRETE VARIABLES CONSIDERING TRANSIENT LOADS. 1–3. https://doi.org/10.7712/140123.10210.19045

Andreassen, E., Clausen, A., Schevenels, M., Lazarov, B. S., & Sigmund, O. (2011). Efficient topology optimization in MATLAB using 88 lines of code. Structural and Multidisciplinary Optimization, 43(1). https://doi.org/10.1007/s00158-010-0594-7

Bendsøe, M. P. (1995). Optimization of Structural Topology, Shape, and Material. In Optimization of Structural Topology, Shape, and Material. Springer Berlin Heidelberg. https://doi.org/10.1007/978-3-662-03115-5

Bendsøe, M. P., & Sigmund, O. (1999). Material interpolation schemes in topology optimization. Archive of Applied Mechanics, 69(9–10). https://doi.org/10.1007/s004190050248

Bendsoe, M. P., & Sigmund, O. (2003). Topology Optimization: Theory, Methods, and Applications. Springer Berlin Heidelberg. https://books.google.com.br/books?id=NGmtmMhVe2sC

Bradley, A. M. (2024). PDE-constrained optimization and the adjoint method 1.

Chickermane, H., & Gea, H. C. (1997). Design of multi-component structural systems for optimal layout topology and joint locations. Engineering with Computers, 13(4), 235–243. https://doi.org/10.1007/BF01200050

Farrell, P. E., Ham, D. A., Funke, S. W., & Rognes, M. E. (2013). Automated Derivation of the Adjoint of High-Level Transient Finite Element Programs. Https://Doi.Org/10.1137/120873558, 35(4). https://doi.org/10.1137/120873558

Ferro, R. M., & Pavanello, R. (2023). Sequential method of topological optimization in multi-component systems. Latin American Journal of Solids and Structures, 20(6). https://doi.org/10.1590/1679-78257576

Ferro, R., & Pavanello, R. (2024). Minimization of Structural Dynamic Compliance in 3D Multicomponent Systems: A Topological Optimization Approach. Proceedings of the 9th International Symposium on Solid Mechanics. https://doi.org/10.26678/ABCM.MECSOL2024.MSL24-0035

Funke, S. W., & Farrell, P. E. (2013). A framework for automated PDE-constrained optimisation. P ACM Trans. Math. Softw. V, N, Article A, 28. https://doi.org/10.1145/0000000.0000000

Hassani, B., & Hinton, E. (1999). Homogenization and Structural Topology Optimization. In Homogenization and Structural Topology Optimization. Springer London. https://doi.org/10.1007/978-1-4471-0891-7

Jiang, T., & Chirehdast, M. (1997). A systems approach to structural topology optimization: Designing optimal connections. Journal of Mechanical Design, Transactions of the ASME, 119(1). https://doi.org/10.1115/1.2828787

Kang, Z., Zhang, X., Jiang, S., & Cheng, G. (2012). On topology optimization of damping layer in shell structures under harmonic excitations. Structural and Multidisciplinary Optimization, 46(1), 51–67. https://doi.org/10.1007/S00158-011-0746-4

Langtangen, H. P., & Logg, A. (2016). Solving PDEs in Python. Solving PDEs in Python. https://doi.org/10.1007/978-3-319-52462-7

Lazarov, B. S., & Sigmund, O. (2011). Filters in topology optimization based on Helmholtz-type differential equations. International Journal for Numerical Methods in Engineering, 86(6). https://doi.org/10.1002/nme.3072

Li, Q., Steven, G. P., & Xie, Y. M. (2001). Evolutionary structural optimization for connection topology design of multi-component systems. Engineering Computations (Swansea, Wales), 18(3–4), 460–479. https://doi.org/10.1108/02644400110387127

Liu, P., & Kang, Z. (2018). Integrated topology optimization of multi-component structures considering connecting interface behavior. Computer Methods in Applied Mechanics and Engineering, 341. https://doi.org/10.1016/j.cma.2018.07.001

Logg, A., Wells, G., & Mardal, K.-A. (2011). Automated solution of differential equations by the finite element method. The FEniCS book. In Lecture Notes in Computational Science and Engineering (Vol. 84). https://doi.org/10.1007/978-3-642-23099-8

Mecias Da, O., & Junior, S. (2017). Otimização topológica em problemas de vibrações harmônicas forçadas utilizando potência de entrada. https://repositorio.ufsc.br/handle/123456789/191045

Menassa, R. J., & DeVries, W. R. (1991). Optimization Methods Applied to Selecting Support Positions in Fixture Design. Journal of Engineering for Industry, 113(4), 412–418. https://doi.org/10.1115/1.2899715

Meng, F., Meng, L., Wang, J., Zhu, J., Wang, B. P., Yuan, S., & Zhang, W. (2024). Topology optimization for minimum dynamic compliance using an antiresonant frequency constraint. Structural and Multidisciplinary Optimization, 67(9), 1–19. https://doi.org/10.1007/S00158-024-03878-9/FIGURES/23

Mitusch, S., Funke, S., & Dokken, J. (2019). dolfin-adjoint 2018.1: automated adjoints for FEniCS and Firedrake. Journal of Open Source Software, 4(38). https://doi.org/10.21105/joss.01292

Moreland, K., Ayachit, U., Geveci, B., Quammen, C., Demarle, D., Moreland, K., Bauer, A., Boeckel, B., Lipsa, D., Westphal, M., Pouderoux, J., Waldon, S., Choudhary, A., Philip, S., Zagaris, G., Loring, B., Maxwell, T., Patchett, J., Ahrens, J., … Sherman, B. (2016). The ParaView Guide. Sandia National Laboratories.

Olhoff, N., & Du, J. (2014). Topological design for minimum dynamic compliance of structures under forced vibration. CISM International Centre for Mechanical Sciences, Courses and Lectures, 549, 325–339. https://doi.org/10.1007/978-3-7091-1643-2_13/COVER

Pedersen, N. L. (2000). Maximization of eigenvalues using topology optimization. Structural and Multidisciplinary Optimization, 20(1), 2–11. https://doi.org/10.1007/S001580050130/METRICS

Qian, Z., & Ananthasuresh, G. K. (2004). Optimal embedding of rigid objects in the topology design of structures. Mechanics Based Design of Structures and Machines, 32(2). https://doi.org/10.1081/SME-120030555

Rakotondrainibe, L., Allaire, G., & Orval, P. (2020). Topology optimization of connections in mechanical systems. Structural and Multidisciplinary Optimization, 61(6). https://doi.org/10.1007/s00158-020-02511-9

Remacle, J., & Geuzaine, C. (2007). Gmsh : a three-dimensional finite element mesh generator with built-in pre- and post-processing facilities What is Gmsh ? INTERNATIONAL JOURNAL FOR NUMERICAL METHODS IN ENGINEERING Int. J. Numer. Meth. Engng, 0.

Rojas-Labanda, S., & Stolpe, M. (2015). Benchmarking optimization solvers for structural topology optimization. Structural and Multidisciplinary Optimization, 52(3), 527–547. https://doi.org/10.1007/S00158-015-1250-Z

Rozvany, G. I. N., Bendsø, M. P., & Kirsch, U. (1995). Layout optimization of structures. Applied Mechanics Reviews, 48(2). https://doi.org/10.1115/1.3005097

Wächter, A., & Biegler, L. T. (2006). On the implementation of an interior-point filter line-search algorithm for large-scale nonlinear programming. Mathematical Programming, 106(1). https://doi.org/10.1007/s10107-004-0559-y

Wang, F., Lazarov, B. S., & Sigmund, O. (2010). On projection methods, convergence and robust formulations in topology optimization. Structural and Multidisciplinary Optimization 2010 43:6, 43(6), 767–784. https://doi.org/10.1007/S00158-010-0602-Y

Xie, Y. M., & Steven, G. P. (1997). Basic Evolutionary Structural Optimization. In Evolutionary Structural Optimization (pp. 12–29). Springer London. https://doi.org/10.1007/978-1-4471-0985-3_2

Zhang, W., Xia, L., Zhu, J., & Zhang, Q. (2011). Some recent advances in the integrated layout design of multicomponent systems. Journal of Mechanical Design, Transactions of the ASME, 133(10). https://doi.org/10.1115/1.4005083

Zhu, J.-H., Guo, W.-J., Zhang, W.-H., & Liu, T. (2017). Integrated layout and topology optimization design of multi-frame and multi-component fuselage structure systems. Structural and Multidisciplinary Optimization, 56(1), 21–45. https://doi.org/10.1007/s00158-016-1645-5